Impact of the aqueous pyrrolidinium hydrogen sulfate electrolyte formulation on transport properties and electrochemical performances for polyaniline-based supercapacitor

Fatima Al-Zohbi, Johan Jacquemin, Fouad Ghamouss, Bruno Schmaltz, Mohamed Abarbri, Khalil Cherry, Mohamad Fadel Tabcheh, François Tran-Van

Contents lists available at ScienceDirect

Journal of Power Sources

journal homepage: www.elsevier.com/locate/jpowsour

Impact of the aqueous pyrrolidinium hydrogen sulfate electrolyte formulation on transport properties and electrochemical performances for polyaniline-based supercapacitor

Fatima Al-Zohbi [a], Johan Jacquemin [a], Fouad Ghamouss [a], Bruno Schmaltz [a], Mohamed Abarbri [a], Khalil Cherry [b], Mohamad fadel Tabcheh [c], François Tran-Van [a]

[a] *Laboratoire de Physico-Chimie des Matériaux et des Electrolytes pour l'Energie (EA 6299), Université de Tours, Parc de Grandmont 37200 Tours, France; alzohbi-fatima@hotmail.com,* jj@univ-tours.fr, *ghamouss@univ-tours.fr, bruno.schmaltz@univ-tours.fr and mohamed.abarbri@univ-tours.fr*

[b] *Laboratoire Matériaux, Catalyse, Environnement et Méthodes Analytiques (MCEMA) Campus Universitaire de Hadath, Liban; Khalil.cherry@ul.edu.lb*

[c] *Laboratoire de chimie appliquée, Faculté des sciences III, Universite Libanaise, Kobbeh - Tripoli – Liban ; mtabcheh@ul.edu.lb*

**Correspondence: francois.tran@univ-tours.fr; Tel.: +33 02 47 36 69 23 (F. TRAN-VAN)*

A B S T R A C T

During this work, the protic ionic liquid (PIL) pyrrolidinium hydrogen sulfate, [Pyrr][HSO_4], is synthesized and its mixture with water is then characterized prior to be used as a potential electrolyte for polyaniline (Pani) based supercapacitors. The transport properties of the [Pyrr][HSO_4] – water binary mixture is determined at three different PIL/water weight ratios (*i.e.* 14/86, 41/59 and 70/30) as a function of the temperature from 5 to 70 °C. In the light of such an analysis, the optimum value of the ionic conductivity, reaching 178 mS/cm at 25 °C, is obtained for the [Pyrr][HSO_4]/water weight ratio close to 41/59. The electrochemical behavior of Pani is then investigated in these electrolytes to further investigate the impact of their formulation on supercapacitor performances. Based on this work, the Pani electrode shows the best electrochemical performances using the electrolyte 41/59 [Pyrr][HSO_4]/water weight ratio leading to a specific capacitance of 380 F/g at 10 mV/s, a low relaxation time constant τ_0 close to 5 s and a gravimetric capacitance retention of 68% after 1000 cycles at 2A/g.

Keywords: Polyaniline (Pani), Protic ionic liquid (PIL), Electrolyte, Supercapacitors

G R A P H I C A L A B S T R A C T

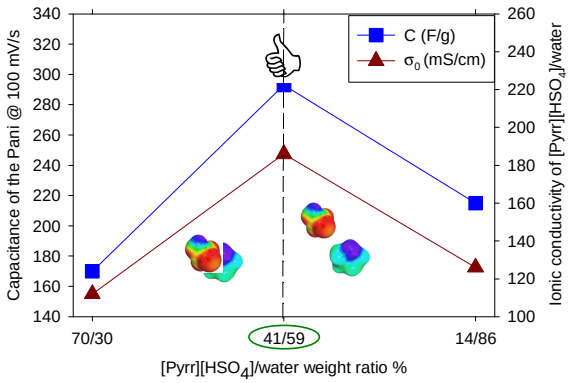

.

1. Introduction

Since the last two decades, the polyaniline (Pani) has attracted a great attention as one of the most performing conducting polymers (CP) to design novel electrode materials for supercapacitors.[1-9] Pani is often characterized by its good thermal stability, high electronic conductivity in its doped state, low cost driven by its simple synthesis,[10] and its high theoretical mass specific capacitance (*ca.* 750 F/g).[11] As other electrode materials for supercapacitors, the electrochemical performances of Pani depend, among several parameters, including the formulation of the electrolyte.[12-14].

Since the last decade, ionic liquids have been widely used as electrolytes for supercapacitor applications.[15-19] This choice is driven by their excellent chemical stability, thermal stability, low vapor pressure and high ionic conductivity.[20, 21] It is well defined in the literature that ionic liquids (ILs) can be classified into different subclasses depending on their structure.[22] The two main subclasses are the aprotic ionic liquids (AILs) and the protic ionic liquids (PILs). The two main differences between these two subclasses are the presence (PILs) or the absence (AILs) of labile hydrogens, and their synthesis costs as PILs are, normally, more easily obtained through a simple proton transfer between an acid and a base of Brönsted.[22]. To date, electrochemical behaviors of Pani have been widely reported in AILs.[23-26] Nevertheless, based on our best knowledge, properties of the Pani have not been yet reported in PIL for charge storage applications, while few other conjugated polymers like polypyrrole, have been characterized in such electrolytes.[27, 28] Due to its specific electroactivity in acidic media, [12, 29-31] Pani can be theoretically studied in electrolytes containing a PIL especially in those containing a PIL dissolved in water to reinforce the hydrogen-bonds network and control the acidity of the solution. Moreover, their simple synthesis and low cost (compare to AILs) justify also the investigation of PILs as potential electrolytes for electrochemical storage devices. For all these reasons, the pyrrolidinium hydrogen sulfate ([Pyrr][HSO_4]) was chosen to probe the feasibility to use PIL as electrolyte in Pani supercapacitors. This selection was also chosen by the fact that this PIL has been already studied by our group as electroplymerization medium able to enhance the electrochemical behavior of conducting polymer (polypyrrole). [27]

The main objective of this work is to study the electrochemical behaviors of Pani in PIL-based aqueous electrolyte for supercapacitor applications. Prior to investigate such electrochemical performances, the [Pyrr][HSO_4]-based PIL has been firstly synthesized, electrolytes containing the [Pyrr][HSO_4] mixed with water have been formulated and then characterized as a function of the temperature and water composition. The influence of water on [Pyrr][HSO_4] density and transport properties (ionic conductivity and viscosity) has been investigated to fine tune the formulation of potential electrolytes for Pani-based supercapacitors. These data have been then discussed in term of interaction changes in solution thanks to collected DFT calculations. Then, the electrochemical behaviors of Pani in these electrolytes have been determined to further examine the impact of the electrolyte formulation on their supercapacitor performances.

2. Experimental Section

2.1. Materials

The aniline used during this work (99.8 %, Acros) was firstly distilled under a reduced pressure before to be used. Sulfuric acid (95-98 %, Alfa Aesar), ammonium persulfate (98 %, Alfa Aesar), chlorhydric acid (57 %, Alfa Aesar), pyrrolidine (≥99 %, Fluka), activated carbon (Norit, Super DLC-50), carbon black (Timcal, super C65) and polytetrafluoroethylene (60 wt% dispersion in H_2O, Aldrich) were used as received.

2.2. Synthesis of the selected Protic Ionic Liquid (PIL)

Pyrrolidinium hydrogen sulfate [Pyrr][HSO_4] was prepared according to the procedure described by Anouti *et al*.[32] Pyrrolidine was introduced in a three-necked round-bottomed flask, which was immerged in an ice bath, and equipped with a reflux condenser, a dropping funnel and a thermometer. Under vigorous stirring, equimolar quantity of sulfuric acid was added dropwise to the pyrrolidine by keeping the reaction temperature under 25 ^{o}C using ice bath. The resulting product was then dried during 2-4 days under vacuum (1 Pa) at room temperature. The residual water content was then quantified by Karl Fisher coulometer titration (831 KF coulometer) as close to 0.15 wt%. The collected [Pyrr][HSO_4] was then a viscous liquid at room temperature.

2.3. Synthesis of the Pani

Pani was prepared by following the synthesis methodology described in the literature.[12, 33] Briefly, 1 g of aniline (0.01 mol) was dissolved in 35 mL of acidic aqueous solution (1 mol/dm^3 HCl) and cooled at 5 °C. Then, ammonium persulfate acidic solution (3.06 g dissolved in 15 mL of 1 mol/dm^3 HCl), cooled at 5 °C using an ice bath for 10 min, was then dropwise added, under stirring, to the above-mentioned aniline solution. By following this experimental protocol, the aniline concentration reaches 0.2 mol/dm^3 in the final solution. The reaction was stirred 24 h at 5 °C. The obtained dark green precipitate was then filtered, washed three times with deionized water and ethanol prior to be dried under vacuum (1 Pa) at 60 °C during 15 h. Synthesis of Pani was then confirmed by using Infra-red (IR) spectroscopy.

Attenuated total reflection infrared (ATR-IR) spectroscopy was then used to confirm the Pani structure by comparing the collected spectrum (Figure S1 of the ESI) with those described already in the literature: [12, 34, 35] showing peaks at 1559 cm^{-1} (quinone ring N=Q=N stretching), 1470 cm^{-1} (benzene rings N-B-N stretching), 1287 cm^{-1} (C-N stretching), 1079 cm^{-1} (C–H in-plane deformation) and 785 cm^{-1} (out-of-plane bending vibration of C-H of benzene rings).

2.4. Preparation of selected electrolytes and physical characterizations

During this work, each electrolyte was simply prepared by mass with an accuracy of ± 1.10^{-4} g using an OHAUS pioneer^{TM} balance by mixing at room temperature known quantities of the PIL and the water by taking into account also the residual water already presents in the dried PIL sample. Three electrolytes were prepared to reach [Pyrr][HSO_4]/water weight ratios of 70/30, 41/59 and 14/86 corresponding to mole fractions of PIL close to 0.199, 0.069 and 0.017, respectively.

The density of each sample was determined by using an Anton Parr digital vibrating tube densitometer (model 60/602, Anton Parr, France) from 15 to 50 °C within ± 0.01 °C. The densitometer was firstly calibrated at all temperatures with degassed water and dehumidified air at atmospheric pressure as recommended by the constructor. The uncertainty of the density values is better than 5×10^{-4} g/cm^3.

Anton Paar rolling-ball viscometer Lovis 2000 M/ME was used to determine the viscosity (η) of the selected electrolytes as a function of temperature from 15 to 50 °C. In both cases, the temperature in the cell was regulated within ± 0.02 °C. The viscosity standard (ASTM Oil

Standard S600 of CANNON, 1053 mPa s at 25 °C) and ultra-pure water were used to calibrate the viscometer. From this study, the uncertainty of reported viscosity measurements did not exceed ± 1 %.

Conductivity measurements were performed by using a biologic instrument as a function of temperature from 5 to 70 °C. The temperature control was ensured within ± 0.01 °C by means of a JULABO thermostated bath. The conductometer was first calibrated with standard solutions of known conductivity (*i.e.* (0.1 and 0.02) mol/dm^3 KCl aqueous solutions). Each conductivity was recorded when its stability was better than 1 % within 2 min, and the uncertainty of reported conductivities did not exceed ± 2 %.

Attenuated total reflection infrared (ATR-IR) spectrum of the Pani was obtained using a Perkin Elmer (spectrum one model). Herein, the reported spectrum is an average of 4 scans between 2000 cm^{-1} and 500 cm^{-1}.

2.5. Electrodes Preparation and electrochemical measurements

All electrochemistry measurements were carried out on a versatile multichannel potentiostat (Biologic S.A) piloted by the EC Lab V10.32 interface at room temperature (*i.e.* 20 °C). For the three electrodes electrochemical studies, the working electrode (WE) was prepared by mixing 60 wt% of active material (polyaniline), 32 wt% of carbon black, and 8 wt% of polytetrafluoroethylene (PTFE) in a minimal amount of ethanol needed using a pestle and mortar to make a homogeneous paste. The obtained paste was then laminated on a glass surface prior to be dried to remove the volatile solvent used. Each WE was then fabricated by pressing the dried paste on stainless steel mesh. The typical mass of paste loading on each WE is close to 1.5 mg/cm^2. Similarly, the counter electrode (CE) was prepared by pressing 7 mg of a paste containing 70 wt% of activated carbon, 20 wt% of carbon black and 10 wt% of PTFE on stainless steel grid under 10 tons pressure. An Ag wire was also used as a pseudo reference electrode. Then using these three electrodes, cyclic voltammograms (CV) were measured in a classical three electrode configuration cell containing selected electrolytes.

Electrochemical performances of the Pani were also assessed through CVs and electrochemical impedance spectroscopy (EIS) measurements using a symmetrical two-electrode configuration cell made from a Teflon Swagelok-type system. In this case, electrodes were prepared by pressing 3 mg of the paste containing 60 wt% of Pani, 32 wt% of carbon black and 8 wt% of PTFE on stainless steel mesh with a diameter of 0.8 cm (6 mg/cm^2). A porous Whatman® membrane (pore diameter Ø = 90 mm) immersed in the selected electrolytes was used as separator. The electrochemical impedance spectroscopy (EIS) measurements of the Pani electrodes were performed in the frequency range between10 mHz and 500kHz at open circuit potential, with an ac amplitude voltage of 10 mV in selected electrolytes.

2.6. Computational methods

The structure of each studied cluster (*i.e.* [Pyrr][HSO_4] + *n* H_2O, with *n* = 0 to 18) was optimized by using the Turbomole 7.0 program package, [36] as described by our group previously. [37] Before their visualization using TmoleX (version 4.1.1), structures were optimized in the gas phase, with a convergence criterion of 10^{-8} Hartree, using DFT calculations combining the Resolution of Identity (RI) approximation [38, 39] within the Turbomole 7.0 program package using the B3LYP function with the def-TZVP basis set.[40-42] The resulting optimized structures were then used as inputs in the COSMOconfX program (version 4.0) to generate the conformers of each species able to be used then in the COSMOthermX software (version C30 17.05, Mixture Option) to determine the lowest energy contact between two identical clusters to extract then an average of the cation – cation distances in solution. TmoleX software was then used to extract distances between cation-anion and cation-cation in each solution by using collected cosmo files.

3. Results and discussion

This manuscript is divided into two main sections. The first part describes the effect of water level on the transport properties and on the $[Pyrr]^+$…$[HSO_4]^-$ distances in solution. The second part gives the electrochemical behavior of Pani in [Pyrr][HSO_4]/water-based electrolyte at three different PIL/water weight ratios (14/86, 41/59 and 70/30).

3.1. Effect of water on the transport properties of [Pyrr][HSO_4]

Conductivity values were firstly discussed, based on data already described in the literature,[43] in order to probe the effect of water on the transport properties of the [Pyrr][HSO_4] and also to pre-select electrolyte-formulations to be further investigated. Figure 1a illustrates results described in the literature for this binary system showing the evolution of the ionic conductivity of the [Pyrr][HSO_4] solution as a function of the water mass fraction (wt%) at 25 °C.[43] One can see that the ionic conductivity of this solution gradually increases with the water content until to reach a maximum value of 186.6 mS/cm at a PIL/water weight ratio of 41/59 (*i.e.* 59 wt% of water) delimiting the region I, prior to decrease (region II) until to reach a value of 0 mS/cm as water is an insulator material. In the region (I), the cation-anion interactions (see Figure 1b), as well as, the viscosity of [Pyrr][HSO_4] decreases by the addition of water. Such phenomena enhance the charge carriers' mobility in the solution leading to an increase of the conductivity of mixture until to reach the optimum conductivity value. However, further water addition (region (II)), decreases the concentration of the charge carriers due to dilution effect cause by the water, driving in fact a clear decrease of the ionic conductivity of the solution.Figure 1b summarizes the ionic conductivity and viscosity values determined herein for [Pyrr][HSO_4]/water electrolytes formulated at three different PIL/water weight ratios *ca.* 14/86, 41/59 and 70/30. These ratios have been selected along with data for the pure PIL as they are localized in the main areas of the curve $\sigma = f$ (water wt%) shown in Figure 1a. One can note that, the collected ionic conductivity and viscosity values at 25 °C are close to (83 mS/cm and 8.7 mPa.s), (178 mS/cm and 2.7 mPa.s) and (109 mS/cm and 1.3 mPa.s) while the following conductivity data 112.80 mS/cm, 186.60 mS/cm and 125.60 mS/cm have been previously reported by Anouti *et al.* [44] for the [Pyrr][HSO_4]/water weight ratio close to 70/30, 41/59 and 14/86, respectively. The difference between data reported in literature and those determined during this work can be explained by the technique used (*i.e.* vibrating tube densitometer: this work and pycnometer: Anouti *et al [44]*), as well as the purity of pristine [Pyrr][HSO_4] such as water level in each sample and/or the presence of unreacted material like the pyrrolidine.

To avoid any further data analysis error associated to the used technique on transport properties of samples, the viscosity and the conductivity of the three selected electrolytes were both measured as a function of the temperature. Collected data are reported in Tables S1 and S2 of the ESI and shown in Figures S1 and S2. As shown in Figures S1-S2, classical temperature dependences on the viscosity and on the conductivity were obtained in each case. The viscosity decreases from (11.8 to 4.7) mPa.s, (3.6 to 1.6) mPa.s, and (1.7 to 0.8) mPa.s from (15 to 50) °C for the solutions containing a [Pyrr][HSO_4]/water weight ratio close to 70/30, 41/59 and 14/86, respectively. In other words, the viscosity of the ([Pyrr][HSO_4] + water) binary mixture decreases by increasing the water composition in solution, as expected. In contrary, the conductivity increases from (52.8 to 149) mS/cm, (134 to 235) mS/cm, and (85.7 to 131) mS/cm from (5 to 70) °C for the solutions containing a [Pyrr][HSO_4]/water weight ratio close to 70/30, 41/59 and 14/86, respectively. As shown in Figure S3 of the ESI, whatever the temperature, the 41/59 [Pyrr][HSO_4]/water weight ratio is more conductive than the two other solutions studied. Furthermore, at low temperature (*i.e.* $T < 55$ °C) it appears than the electrolyte based on the 70/30 [Pyrr][HSO_4]/water weight ratio is less conductive than the 14/86 one. However, at higher temperature this opposite trend was observed. This cross-over is explained by the difference in the number of ions in solution between these two electrolytes and by the large decrease of the viscosity differences between these two electrolytes when the temperature increases (see Figure S2 of the ESI). To further understand the variation of the conductivity as a function of the composition in solution shown in Figure 1a, DFT calculations have been carried-out to investigate the distance between the $[Pyrr]^+$ cation and $[HSO_4]^-$ anion in solution as a function of the water molecules surrounding this PIL. For this study, one molecule of PIL was mixed with up to 18 water molecules and COSMOthermX software was then used to determine the best contact between two identical clusters (*i.e.* [Pyrr][HSO_4] + n H_2O, with n = 0 to 18) to determine then the minimum distance between cation – cation as the function of the water molecules in solution. Results of this study are reported in Table 1 and visualized in Figure S4 of the ESI.

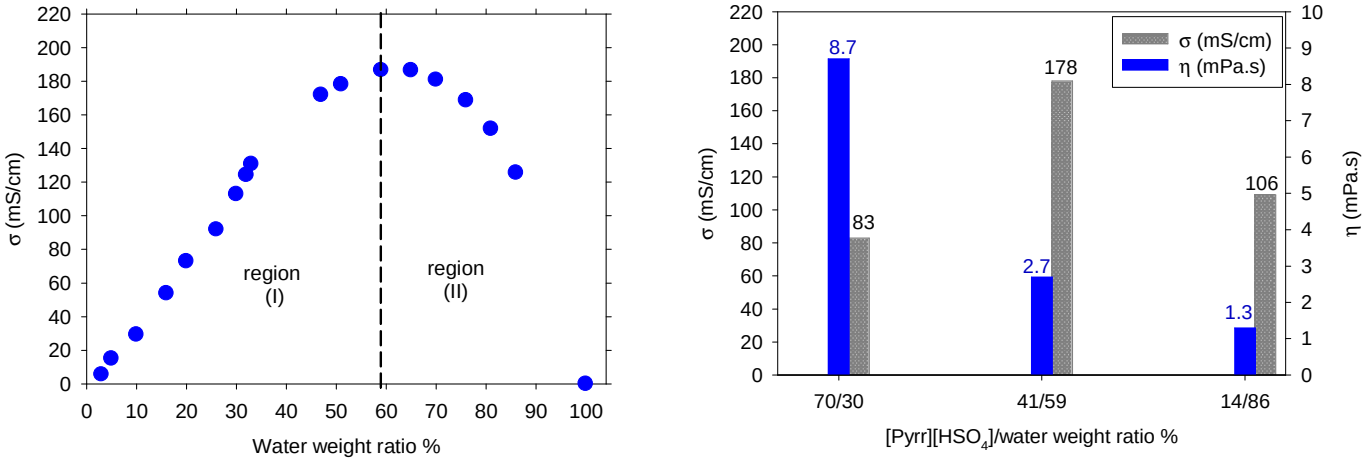

Figure 1. a) Evolution of the conductivity of the [Pyrr][HSO_4] as a function of water content expressed in PIL/water weight ratio based on literature data reported at 25 °C in ref [44] and b) conductivity and viscosity values of selected electrolytes determined during work at 25 °C.

Table 1: Effect of water content on ion distances in solution.

[Pyrr][HSO_4] + *n* H_2O	0	1	2	3	4
C^+…A^- distance /Å	1.710	1.711	1.713	1.711	1.724
C^+…C^+ distance /Å	7.548	8.422	9.109	9.429	9.702
[Pyrr][HSO_4] + *n* H_2O	5	6	7	8	9
C^+…A^- distance /Å	1.783	1.782	1.779	1.814	1.806
C^+…C^+ distance /Å	9.922	10.194	10.890	11.702	11.855
[Pyrr][HSO_4] + *n* H_2O	10	11	12	13	14
C^+…A^- distance /Å	1.811	1.809	3.793	3.835	3.791
C^+…C^+ distance /Å	12.455	12.58	12.911	13.554	13.752
[Pyrr][HSO_4] + *n* H_2O	15	16	17	18	
C^+…A^- distance /Å	3.819	3.801	3.823	3.834	
C^+…C^+ distance /Å	13.856	14.324	14.487	14.676	

Results from DFT calculations reported in Table 1 clearly show that 12 water molecules are requested to break-down H-bond interaction between the $[Pyrr]^+$ cation and $[HSO_4]^-$ anion in solution corresponding to a [Pyrr][HSO_4]/water weight ratio close to 45/55 (*ca.* w_{H2O} = 0.5496). One can appreciate that this value is close to the composition leading to the maximum of conductivity shown in Figure 1a. Furthermore, it appears also that the distance between two cations in solution seems to increase linearly with the number of water molecules as it may be expected by considering solely the effect of the PIL dilution in solution (see Figure S4 of the ESI). On the one hand, in the case of [Pyrr][HSO_4] + *n* H_2O, with $1 \leq n \leq 11$ clusters, strong interactions between the $[Pyrr]^+$ cation and $[HSO_4]^-$ anion (with a cation-anion distance increasing from 1.71 Å to 1.81 Å with *n* = 1 to 11 water molecules) are still observed, which seems to be comparable to that observed in the case of the pure PIL (1.71 Å) while the conductivity increase could be attributed to a Grotthuss mechanism in solution as claimed by Anouti *et al.* [32] On the other hand, in the case of [Pyrr][HSO_4] + *n* H_2O, with *n* > 12 clusters, weaker interactions between the $[Pyrr]^+$ cation and $[HSO_4]^-$ anion are then observed (with a cation-anion distance increasing from 3.80 Å to 3.83 Å with *n* = 12 to 18 water molecules) while the conductivity increase could be attributed to a combination of Grotthuss- and vehicle-type mechanisms,[32] until reaching the maximum of conductivity (for n = 12) (*i.e.* a well-balanced distances between all ions in solution) prior to decrease due to dilution effect by adding more water molecules. Classical Walden rule, $\Lambda \cdot \eta = C$, was then used to further

support DFT calculations. Briefly, Walden rule is based on a potential inverse relationship between the viscosity and conductivity of a given electrolyte.[45] This can be represented with the use of a Walden plot; a plot of $\log(\eta^{-1})$ *vs.* $\log(\Lambda)$, where the reciprocal viscosity (or fluidity, η^{-1}) is given in $Poise^{-1}$ and the molar conductivity, Λ, is given in $S \cdot cm^2/mol$. The derived Λ values for each electrolyte at 25 °C are provided in Table 2, along with the Walden product, C. The Walden plots within the temperature range of 15 – 50 °C for the tested electrolytes are shown in Figure S5 of the ESI. Herein the viscosity and conductivity of each electrolyte at a given temperature is calculated by accurate interpolation of VTF correlations with parameters provided in the ESI and the molar conductivity is calculated by division of electrolytic conductivity by the PIL concentration [$\Lambda = \sigma$ (S/cm)/concentration (mol/cm^3)]. The PIL concentration in solution was calculated by linear interpolation of the temperature-dependency of the solution density, PIL weight fraction in solution and the IL molecular weight [concentration = $w_{PIL} \times \rho$ (g/cm^3) / M (g/mol)]. The calculated values for Λ and η^{-1} over a temperature range of 15 – 50 °C are presented in Table S3 in the ESI.

Table 2: Density, ρ; conductivity, σ; derived molar conductivity, Λ; viscosity, η; and Walden product, C at 25 °C for each electrolyte.

PIL/water	ρ (g/cm^3)	σ (S/cm^1)	c_{ion} (mol/cm^3)	Λ ($S.cm^2/mol$)	η (P)	C ($P.S.cm^2/mol$)
14/86	1.0509	0.1094	0.000830	131.78	0.0132	1.73
41/59	1.1506	0.1785	0.002662	67.05	0.0271	1.81
70/30	1.2606	0.0823	0.004980	16.58	0.0869	1.44

3.1. Electrochemical performances of the Pani in selected electrolytes

The selected binary mixtures [Pyrr][HSO_4]/water (weight ratios of 14/86, 41/59 and 70/30) were used as electrolytes for supercapacitors based on Pani electrodes. The electrochemical measurements were conducted in a three-electrode cell configuration as well as, in a symmetric two-electrode cell configuration.

3.2.1. three-electrode cell configuration

Electrochemical performances of Pani were firstly carried out by cyclic voltammetry using a three-electrode cell to identify the relationship between the redox process of the Pani and the transport properties of PIL-based electrolytes. For comparison, Pani performances have also been studied in the conventional electrolyte (1 mol/dm^3 H_2SO_4). **Figure 2** shows the cyclic voltamogrammes (CV) in each electrolyte from -0.65 to 0.35 V *vs.* NHE at a scan rate of 5 mV/s. As one can see, the current intensity of the CV curves in selected aqueous electrolytes is higher than that obtained in the neat [Pyrr][HSO_4], indicating a higher specific capacitance using the [Pyrr][HSO_4]/water electrolytes. To the best of our knowledge, there is not yet any study discussing the electrochemical performances of Pani in PIL-based electrolyte for supercapacitor applications. However, the relationship between the addition of organic solvent in an AIL-based electrolyte and the electrochemical capacitance of Pani has been reported in the literature [25]. The result is that the mixture electrolytes of 1-methyl-3-butylimidazolium hexafluorophosphate and acetonitrile could improve the electrochemical capacitance and cycle life of Pani compared to achievable results in pristine AIL. The addition of acetonitrile reduces the viscosity and increases the ion dissociation, and therefore enhances the conductivity of the resulting electrolyte. When adding acetonitrile, the electrolyte anion are thus solvated before incorporation into polymer, this can explain the enhancement of Pani electrochemical results. [25]. It should be noted that the addition of organic solvent such as acetonitrile (flammable, volatile and toxic) in AILs can has a negative effect on the environmental friendly benefits and safety properties of AILs. On this basis, we can ascribe the low current intensity of the CV curve in the neat [Pyrr][HSO_4] to the low ionic conductivity (5.5 mS/cm given in [43]) and the high viscosity (200 mPa.s given in [43]) at 20 °C of the neat PIL comparing to those achieved for selected PIL aqueous electrolytes.

Furthermore, each CV curve presents a redox couple (Figure 2). The latter is attributed to the redox transition of Pani between a semiconducting state (leucoemeraldine form) and a conducting state (emeraldine form).[46] The “reversibility” of the redox reaction is estimated as the difference between the potential of the oxidation and reduction peaks (denoted $\Delta E_{O,R}$). [47] Herein, $\Delta E_{O,R}$ values are close to 0.68, 0.60 and 0.52 V at 5 mV/s

by using the [Pyrr][HSO_4]/water weight ratios of 70/30, 14/86 and 41/59, which have a Walden product of 1.44, 1.73 and 1.81 P.s.cm^2/mol, respectively, In fact, one can appreciate that $\Delta E_{O,R}$ value could be related to the Walden product of the electrolyte. In other words, the electrolyte based on the 41/59 PIL/water weight ratio, which has a higher Walden product (1.81 P.s.cm^2/mol), give rise to fast reversible doping process of the Pani similar to the conventional reference electrolyte (H_2SO_4 1mol/dm^3) ($\Delta E_{O,R}$ = 465 mV). In contrast, the CV curves obtained using Pyrr][HSO_4]/water show a larger responsive gravimetric current density than that realized in the conventional electrolyte (1 mol/dm^3 H_2SO_4), which indicate larger gravimetric capacitances especially for the optimized formulation Pyrr][HSO_4]/water 41/59. Moreover the acidity of the solution of Pyrr][HSO_4]/water are much lower than the one of 1 mol/dm^3 H_2SO_4. A limitation in term of corrosion of aluminum current collectors should be particularly interesting for industrial developments.

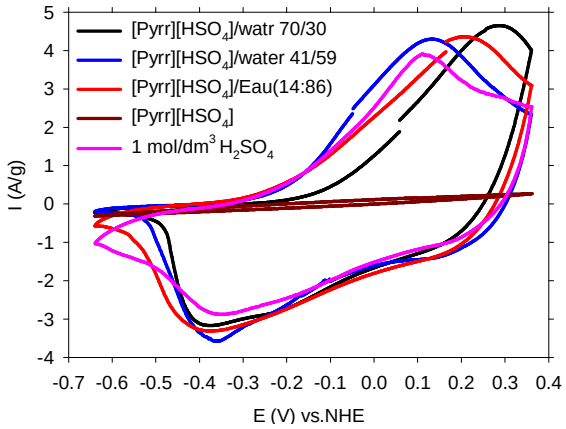

Figure 2. CV curves for the Pani in 1 mol/dm^3 H_2SO_4, the neat [Pyrr][HSO_4] (*i.e.* containing 1.5 wt % of water) and in selected [Pyrr][HSO_4]/water electrolytes at 5 mV/s.

3.2.2. Symmetric two-electrode configuration

Electrochemical properties of the Pani were then determined using a symmetric two-electrode test configuration to truly evaluate the real performances of Pani in [Pyrr][HSO_4]/water electrolytes formulations, and so to understand the relationship electrolyte transport properties-Pani performances **Figure 3** presents the CV curves of the Pani recorded at scan rates of 100 and 15 mV/s in a potential window of 0.8 V. The CV curves exhibit a rectangular shape with a deformation depending on the electrolyte medium. Redox peaks are also present in the CV curves recorded at low scan rate (**Figure 3**b). These features reveal the faradaic capacitive behavior of the supercapacitors [48]. The area of CV curve obtained using the [Pyrr][HSO_4]/water weight ratio of 41/59 is higher than those obtained for the two other studied electrolytes, indicating a more important quantity of charge exchanged per unit of mass of electroactive materials. This result can be linked to the fact that this specific electrolyte is corresponding to the optimum of the ionic conductivity (178 mS/cm) and has a low viscosity (2.7 mPa.s). According to the Table 2 and Figure 3, one can clearly see that the electrolyte formulation affects not only the transport properties of the electrolyte but more importantly the Pani electroactivity and thus the supercapacitor performances.

Then the values of the specific capacitance were calculated from the discharge curves based on the mass of active materials using the following equation (eq. 1):

$$C = \frac{\int I dt}{m\ x\ \Delta V} \qquad \text{(eq. 1)}$$

where *C* is the specific capacitance of the active materials of both electrodes (F/g), *I* is the constant discharge current (mA), *dt* is the discharge time (s), *ΔV* is the voltage difference in discharge (V) and *m* is the total mass of the active material onto both electrodes (mg). Obtained capacitance values are then multiplied by 4 to reach specific capacitance per electrode mass. The discharge specific capacitance values plotted

against scan rate are shown in **Figure 3c.** At a high scan rate of 100 mV/s, the specific capacitance of the Pani is 293, 215 or 170 F/g in [Pyrr][HSO_4]/water weight ratio of 41/59, 14/86 or 70/30, respectively. As we can see, the higher specific capacitance of the Pani is obtained in [Pyrr][HSO_4]/water weight ratio of 41/59, which has the maximum ionic conductivity (Figure 1a) and weaker H-bond interaction between the $[Pyrr]^+$ cation and $[HSO_4]^-$ anion in solution (DFT calculation), indicating the facility of the incorporation/expulsion of the ions into/out of the Pani. The specific capacitance of the Pani increases with decreasing the scan rate, as expected [48], to reach 360, 381 and 311 F/g in 14/8, 41/59 and 70/30 [Pyrr][HSO_4]/water solution at 10 mV/s, respectively. Therefore, one can conclude that the influence of the electrolyte formulation (*i.e.* driven by its ionic conductivity and viscosity) on the capacitance of the Pani is a key factor as confirmed by increasing the scan rate from 15 to 100 mV/s and by comparing then the relative decrease of the capacitance. However, such a decrease seems to be lower (23 %) using the 41/59 [Pyrr][HSO_4]/water electrolyte that those observed, *e.g.* 41 % and 46 %, using the 14/86 and 70/30 solutions, respectively (**Figure 3**d). CV of symmetric Pani/Pani devices in H_2SO_4 have also been realized and compared to the ones in PIL/water formulations. It can be conclude that the specific capacitances are higher when using [Pyrr][HSO_4] whatever the scan rate (in the range 10-100 mV/s) . At 100 mV/s, the capacitance is even twice as high in [Pyrr][HSO_4]/water 41/59 as in 1 mol/dm^3 H_2SO_4. The retention of capacitance when the scan rate increases is also improved which confirm a better ion transport kinetic in [Pyrr][HSO_4] media. (figure 3c and 3d).

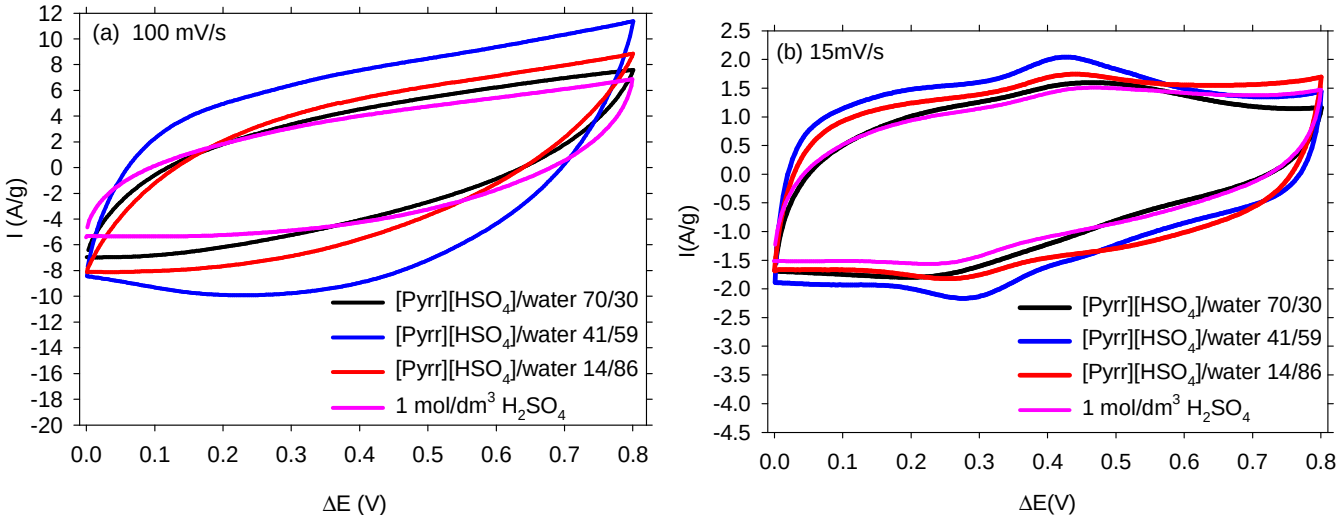

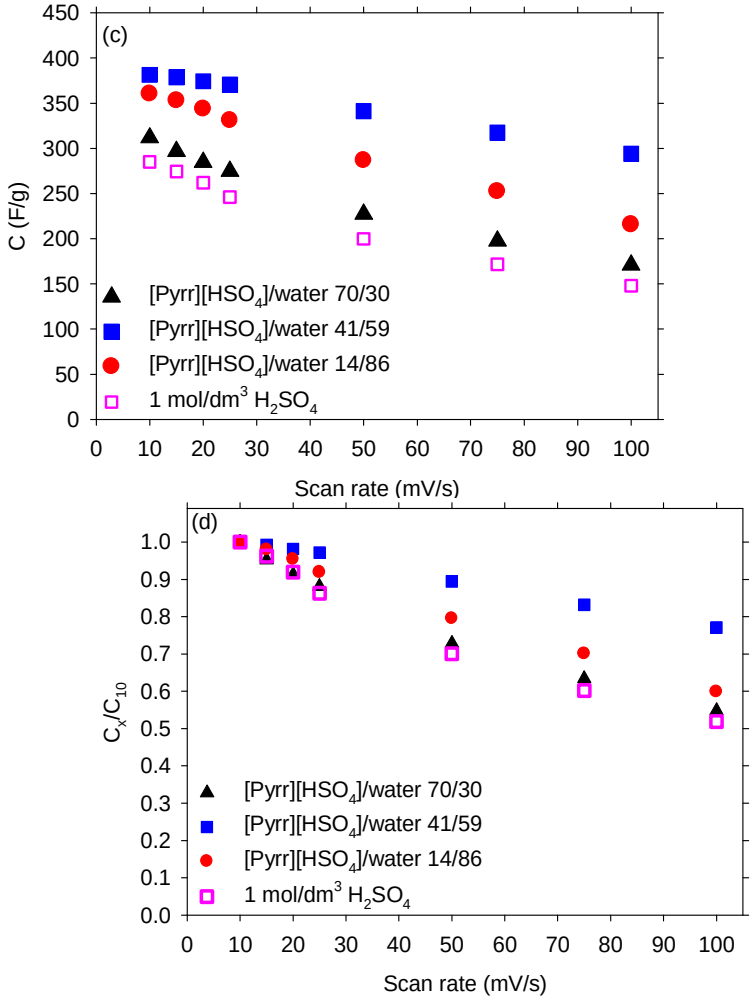

Figure 3. CV curves at scan rate of 100 mV/s (a) and 15 mV/s (b) for the Pani, specific capacitance (c) and capacitance retention as a function of the scan rate for the Pani (d) in 1 mol/dm^3 H_2SO_4 and in selected [Pyrr][HSO_4]/water electrolytes at different PIL/water weight ratios (70/30, 41/59 and 14/86). (where C_x and C_{10} are the specific capacitance at x and 10 mV/s, respectively).

The energy density and the power density are estimated from the CV using the equations 2 and 3 [49], respectively. Where E, C, ΔV, P and t are, respectively, average energy density (Wh/kg), specific capacitance of the device (F/g), potential window of discharge (V), average power density (W/kg) and discharge time (h). Ragone plot of the Pani at different scan rate using 1 mol/dm^3 H_2SO_4 or [Pyrr][HSO_4]/water 59/41 as electrolyte is shown in Figure 4. As one can see, the energy densities reduce with increasing power densities in both investigated electrolytes. For Pani investigated in [Pyrr][HSO_4]/water 59/41, the energy density can reach 8.5 Wh/kg at a power density of almost 400 W/kg, and still remains 6.5 Wh/kg at a power density of around 3000 W/kg. However, for Pani studied in 1 mol/dm^3 H_2SO_4, the energy density decreases from 6.3 to 3.3 Wh/kg when the power density increases from 285 to around 1500 W/kg. At a specific energy of 6.3 Wh/kg, the specifi power in more than time times higher in the PIL formulation. This result indicates that [Pyrr][HSO_4]/water 59/41 can be a good alternative for the conventional electrolyte (H_2SO_4) for increasing as well as specific energy and power of the device.

$$E = \frac{1}{2} C(\Delta V^2) \qquad \text{(eq. 2)}$$

$$P = \frac{E}{t} \qquad \text{(eq. 3)}$$

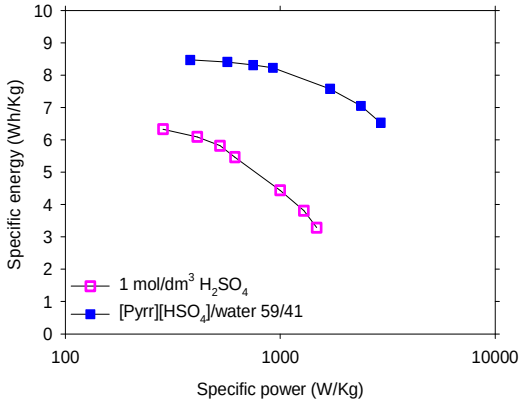

Figure 4: Ragone plot of the Pani using 1 mol/dm^3 H_2SO_4 or [Pyrr][HSO_4]/water 59/41 as electrolyte

Pani-based supercapacitors have been then characterized by EIS to further evaluate the properties of the charge transport in the Pani//electrolyte interface as a function of the electrolyte formulation. Figure 5 shows the Nyquist plots and the magnification of the high frequency range (the insert). As expected, all Nyquist plots are described by a semi-circle (high frequencies), a 45º sloping line (middle frequency) and a straight line (low frequencies). [50] At a high frequency (500 kHz), the intercept of the Nyquist plot with the real axis corresponds to the ionic resistance of the device (R_s). The R_s values are 0.43, 0.56 and 0.78 Ω using the [Pyrr][HSO_4]/water weight ratio of 41/59, 14/86 and 70/30, having an ionic conductivity close to 178, 106 and 83 mS/cm, respectively. It can be noted that the order of R_s values of the devices in selected electrolytes are opposite to that of the ionic conductivity values of electrolytes, as expected.[51, 52]. The semi-circle diameter is generally attributed to the charge-transfer resistance R_{ct} of the electrode in the high frequency range. In other words, the 41/59 electrolyte seems to display the best interface properties with the Pani electrode associated to the lowest Rct. In the low frequency region, the vertical line indicates an ideal capacitive behavior.[53] Furthermore, a line nearly parallel to the imaginary axis reveals a short ion diffusion path and fast ion diffusion rate close to a pure capacitive behavior.[53]. According to data plotted in Figure 5, the faster ions diffusion rate is observed in the 41/59 [Pyrr][HSO_4]/water electrolyte.

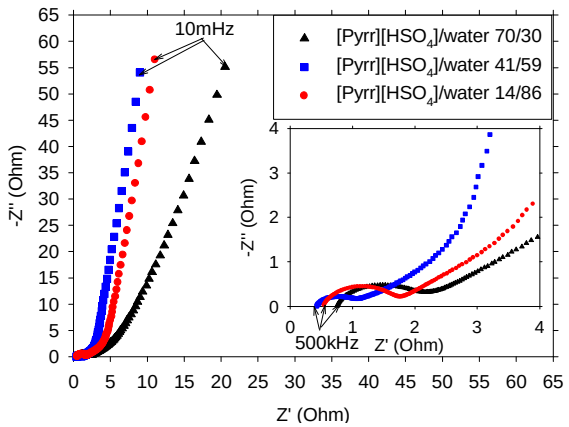

Figure 5. Nyquist plots of the Pani in selected electrolytes at open circuit potential between 10 mHz and 500 kHz. Inset plot shows the magnification of the high frequency range for Pani in selected electrolytes.

The impedance of the Pani based pseudocapacitors was then studied in terms of complex capacitance using the complex model of the capacitance. The complex capacitance investigates the evolution of the capacitance *vs.* the frequency.[51] The real part C'(ω) and the imaginary part C"(ω) of the capacitance are calculated according to the below equations (eq. 2 and eq. 3):

$$C'(\omega) = \frac{-Z''(\omega)}{\omega\,|Z(\omega)|^2} \qquad \text{(eq. 2)}$$

$$C''(\omega) = \frac{-Z'(\omega)}{\omega\,|Z(\omega)|^2} \qquad \text{(eq. 3)}$$

Where ω is the angular frequency ($2\pi\phi$), $Z(\omega)$ is the complex impedance, Z' (ω) and $Z''(\omega)$ are the real and imaginary part of the complex impedance, respectively. Then C' and C" are plotted *vs.* the frequencies and shown in Figure 6.

As shown in **Figure 6a**, the evolution of the real part of capacitance (C′) against the frequency seems to be similar for Pani in all investigated electrolytes. Furthermore, at high frequency, one can see a purely resistive behavior (phase angle is around 0 °). The C' increases when the frequency decreases (between 1 Hz and 10 mHz. The C′ of Pani in selected [Pyrr][HSO_4]/water electrolytes follows the same order than that observed for CVs results (**Figure 3**c). In the case of the C″ values *vs.* frequency plots (**Figure 6b**), one can observe, as expected, a maximum which separates the resistive behavior at high frequencies and the capacitive behavior at low frequencies. The maximum of C" corresponds to a relaxation frequency f_0 related to a relaxation time constant τ_0 ($\tau_0 = 1/f_0$). The time constants τ_0 of the devices (symmetrical electrodes of 6 mg/cm^2) are close to 33, 10 and 5 s by using the 70/30, 14/86 and 41/59 [Pyrr][HSO_4]/water electrolytes, respectively, which could be compared to the literature value reported for Pani/carbon materials (~ 6.25 s for 2.47 mg/cm^2 in 1 mol/dm^3 H_2SO_4) [54].

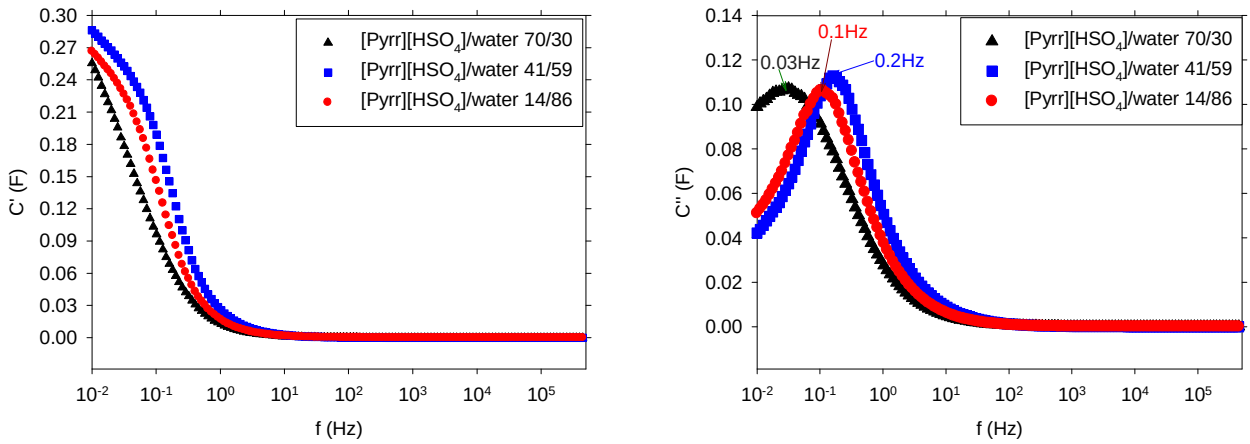

Figure 6. a) Real part of the capacitance (C') and b) imaginary part of the capacitance (C") *vs.* the frequency of the Pani in selected [Pyrr][HSO_4]/water electrolytes.

In the light of all results obtained, we then decided to determine the cycle stability of the Pani in the [Pyrr][HSO_4]/water weight ratio of 41/59, which showed the best performances among the two other electrolytes, by using the charge/discharge galvanostatic measurements over 1000 cycles at a current density of 2A/g. As display in the Figure 7a, the charge/discharge cycle presents nonlinear shape implying a pseudocapacitive behavior of the Pani in the investigated electrolyte. The specific capacitance (C) based on electroactive materials as a function of cycle number, as well as, coulombic efficiency are shown in

Figure 7b. The coulombic efficiency (η), which quantifies the efficiency of electron transfer in electrochemical system, is close to 97.9 % for the first cycle. It then rises to about 99.5 % after 20 cycles and still remains constant even after 1000 cycles. The specific capacitance reaches 252 F/g on the initial discharge then decreases down to 169 F/g after 1000 cycles. Therefore, the retention of capacitance is about 68 % in [Pyrr][HSO_4]/water weight ratio 41/59, while it is better than that reported in the literature using the conventional electrolyte 1 mol/dm^3 H_2SO_4 (See Table S4 of the ESI). It is described that the use of AILs as electrolyte enhances the cycle life of Pani based electrode materials but gives rise to a lower capacitance compared to classical aqueous electrolytes [24, 55-57]. The cycle life improvement is attributed to the intrinsic stability of ionic liquid and a better stability of the polymer during its doping-dedoping in the redox process [24, 55, 56]. Therefore, [Pyrr][HSO_4]/water weight ratio 41/59 improves the cycle life as well as the electrochemical performance of Pani based electrode compared to usual aqueous acidic electrolytes (like H_2SO_4).

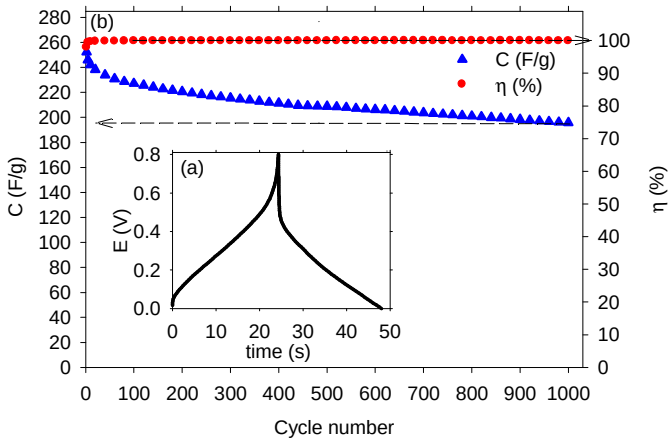

Figure 7. a) First galvanostatic charge/discharge cycle and b) specific capacitance (C) and columbic efficiency (η) of the Pani as a function of cycle number in the 41/59 [Pyrr][HSO_4]/water electrolyte at 2 A/g

4. Conclusions

This manuscript reports on the application of PIL-based electrolyte for supercapacitors based on Pani electrodes. We investigated three different [Pyrr][HSO_4]/water binary mixtures (*i.e.* 14/86, 41/59 and 70/30 [Pyrr][HSO_4]/water wt% ratio). These ratios are localized in the main areas of the curve $\sigma = f$ (water wt%). The electrolyte based on the 41/59 PIL/water presents better transport properties ability than the two others. Furthermore, DFT calculations show that the H-bond interaction between the $[Pyrr]^+$ cation and $[HSO_4]^-$ anion break-down in solution corresponding to a 45/55 [Pyrr][HSO_4]/water weight ratio close to the composition leading to the maximum of conductivity (weight ratio of 41/59).

Electrochemical performances of Pani in the selected electrolyte reveal that the “reversibility” of the redox reaction of Pani could be related to the Walden product of the electrolyte. The fast reversible doping process of the Pani ($\Delta E_{O,R}$ is about 0.52 V at 5 mV/s), the higher specific capacitance (380 F/g at 10 mV/s) of the Pani is obtained in Pyrr][HSO_4]/water weight ratio of 41/59. The EIS measurements confirm the results obtained using cyclic voltammetry. The time constants τ_0 is close to 5 s by using the 41/59 [Pyrr][HSO_4]/water electrolyte showing that this formulation should deliver the highest power efficiency in supercapacitor devices. Furthermore, cycle performances of symmetric redox supercapacitor based on Pani (capacitance retention of 68 % and a coulombic efficiency of 99.5 % for 1000 cycles) are improved using Pyrr][HSO_4]/water weight ratio of 41/59, which has a higher Walden product (1.81 P.s.cm^2/mol), give rise to fast reversible doping process of the Pani.

To conclude, the performances of Pani in the electrolyte containing the 41/59 [Pyrr][HSO_4]/water wt% ratio clearly demonstrate that this PIL-based electrolyte can improve the cycle life as well as the electrochemical performances of Pani based supercapacitors.

Acknowledgments

We gratefully acknowledge RESCOLL-French Research Company and the Lebanese University for their financial support. JJ and FG like to gratefully acknowledge the funding from the regional council “Région Centre” for the DESLIS and S2EA projects.

Appendix A. Supplementary data

References

[1] G.K. Veerasubramani, K. Krishnamoorthy, S. Radhakrishnan, N.-J. Kim, S.J. Kim, J. Ind. Eng. Chem. 36 (2016) 163-168.

[2] X. Li, Y. Liu, W. Guo, J. Chen, W. He, F. Peng, Electrochim. Acta 135 (2014) 550-557.

[3] A. Chellachamy Anbalagan, S.N. Sawant, Polymer 87 (2016) 129-137.

[4] S. Bhandari, D. Khastgir, Mater. Lett. 135 (2014) 202-205.

[5] M.B. Gholivand, H. Heydari, A. Abdolmaleki, H. Hosseini, Mater. Sci. Semicond. Process. 30 (2015) 157-161.

[6] X. Wang, D. Liu, J. Deng, X. Duan, J. Guo, P. Liu, RSC Adv. 5 (2015) 78545-78552.

[7] N.H. Khdary, M.E. Abdesalam, G. El Enany, J. Electrochem. Soc. 161 (2014) G63-G68.

[8] G. Wang, L. Zhang, J. Zhang, Chem. Soc. Rev. 41 (2012) 797-828.

[9] R. Ramya, R. Sivasubramanian, M.V. Sangaranarayanan, Electrochim. Acta 101 (2013) 109-129.

[10] S. Bhadra, D. Khastgir, N.K. Singha, J.H. Lee, Prog. Polym. Sci. 34 (2009) 783-810.

[11] G.A. Snook, P. Kao, A.S. Best, J. Power Sources 196 (2011) 1-12.

[12] S. Chaudhari, Y. Sharma, P.S. Archana, R. Jose, S. Ramakrishna, S. Mhaisalkar, M. Srinivasan, J. Appl. Polym. Sci. 129 (2013) 1660-1668.

[13] H. Zhu, S. Peng, W. Jiang, Sci. World J. 2013 (2013) 8.

[14] T.N. Myasoedova, E.N. Shishlyanikova, T.A. Moiseeva, M. Brzhezinskaya, Adv. Mater. Lett. 7 (2016) 441-444.

[15] A. Balducci, R. Dugas, P.L. Taberna, P. Simon, D. Plee, M. Mastragostino, S. Passerini, J. Power Sources 165 (2007) 922-927.

[16] C. Arbizzani, M. Biso, D. Cericola, M. Lazzari, F. Soavi, M. Mastragostino, J. Power Sources 185 (2008) 1575-1579.

[17] M. Salanne, Topics in Current Chemistry 375 (2017) 63.

[18] M. Armand, F. Endres, D.R. MacFarlane, H. Ohno, B. Scrosati, Nat Mater 8 (2009) 621-629.

[19] A. Brandt, S. Pohlmann, A. Varzi, A. Balducci, S. Passerini, MRS Bulletin 38 (2013) 554-559.

[20] J. Lu, F. Yan, J. Texter, Prog. Polym. Sci. 34 (2009) 431-448.

[21] C. Zhong, Y. Deng, W. Hu, J. Qiao, L. Zhang, J. Zhang, Chem. Soc. Rev. 44 (2015) 7484-7539.

[22] H. Ohno, Koganei, Tokyo,Japan (2011).

[23] E. Naudin, H.A. Ho, L. Breau, D. Belanger, ACS Symp. Ser. 832 (2003) 52-58.

[24] K. Wang, J. Huang, Z. Wei, J. Phys. Chem. C 114 (2010) 8062-8067.

[25] Z. Jun-Ling, Z. Xiao-gang, X. Fang, H. Feng-Ping, J. Colloid Interface Sci. 287 (2005) 67-71.

[26] W. Lu, A.G. Fadeev, B. Qi, E. Smela, B.R. Mattes, J. Ding, G.M. Spinks, J. Mazurkiewicz, D. Zhou, G.G. Wallace, D.R. MacFarlane, S.A. Forsyth, M. Forsyth, Science 297 (2002) 983-987.

[27] M. Porcher, C. Esnault, F. Tran-Van, F. Ghamouss, J. Appl. Electrochem. 46 (2016) 1133-1145.

[28] R.A. Fernández, T.M. Benedetti, R.M. Torresi, J. Electroanal. Chem. 737 (2015) 23-29.

[29] R. Prakash, J. Appl. Polym. Sci. 83 (2002) 378-385.

[30] L. Zhao, L. Zhao, Y. Xu, T. Qiu, L. Zhi, G. Shi, Electrochim. Acta 55 (2009) 491-497.

[31] W.S. Huang, B.D. Humphrey, A.G. MacDiarmid, J. Chem. Soc., Faraday Trans. 1 82 (1986) 2385-2400.

[32] M. Anouti, P. Porion, C. Brigouleix, H. Galiano, D. Lemordant, Fluid Phase Equilib. 299 (2010) 229-237.

[33] E.C. Gomes, M.A.S. Oliveira, Am J Polym Sci 2 (2012) 5-13.

[34] J. Li, X. Tang, H. Li, Y. Yan, Q. Zhang, Synth. Met. 160 (2010) 1153-1158.

[35] W. Yin, E. Ruckenstein, Synth. Met. 108 (2000) 39-46.

[36] R. Ahlrichs, M. Bär, M. Häser, H. Horn, C. Kölmel, Chem. Phys. Lett. 162 (1989) 165-169.

[37] E. Coadou, P. Goodrich, A.R. Neale, L. Timperman, C. Hardacre, J. Jacquemin, M. Anouti, Chem. Phys. Chem. 17 (2016) 3992-4002.

[38] F. Weigend, M. Häser, Theor. Chem. Acc. 97 (1997) 331-340.

[39] F. Weigend, M. Häser, H. Patzelt, R. Ahlrichs, Chem. Phys. Lett. 294 (1998) 143-152.

[40] A.D. Becke, Phys. Rev. A 38 (1988) 3098-3100.

[41] C. Lee, W. Yang, R.G. Parr, Phys. Rev. B 37 (1988) 785-789.

[42] S. Grimme, J. Comput. Chem. 27 (2006) 1787-1799.

[43] M. Anouti, J. Jacquemin, P. Porion, J. Phys. Chem. B 116 (2012) 4228-4238.

[44] M. Anouti, M. Caillon-Caravanier, Y. Dridi, J. Jacquemin, C. Hardacre, D. Lemordant, J. Chem. Thermodyn. 41 (2009) 799-808.

[45] C.A. Angell, Science 267 (1995) 1924-1935.

[46] W. Feng, Q. Zhang, Y. Li, Y. Feng, J. Solid State Electrochem. 18 (2014) 1127-1135.

[47] J. Yan, T. Wei, Z. Fan, W. Qian, M. Zhang, X. Shen, F. Wei, J. Power Sources 195 (2010) 3041-3045.

[48] P.A. Basnayaka, M.K. Ram, E.K. Stefanakos, A. Kumar, Electrochimica Acta 92 (2013) 376-382.

[49] J. Yan, T. Wei, B. Shao, Z. Fan, W. Qian, M. Zhang, F. Wei, Carbon 48 (2010) 487-493.

[50] R. Malik, L. Zhang, C. McConnell, M. Schott, Y.-Y. Hsieh, R. Noga, N.T. Alvarez, V. Shanov, Carbon 116 (2017) 579-590.

[51] P.L. Taberna, P. Simon, J.F. Fauvarque, J. Electrochem. Soc. 150 (2003) A292-A300.

[52] K.S. Ryu, K.M. Kim, N.-G. Park, Y.J. Park, S.H. Chang, J. Power Sources 103 (2002) 305-309.

[53] F. Ke, Y. Liu, H. Xu, Y. Ma, S. Guang, F. Zhang, N. Lin, M. Ye, Y. Lin, X. Liu, Comp. Sci. Technol. 142 (2017) 286-293.

[54] E. Tomšík, I. Ivanko, O. Kohut, J. Hromádková, ChemElectroChem 4 (2017) 2884-2890.

[55] P.C. Innis, J. Mazurkiewicz, T. Nguyen, G.G. Wallace, D. MacFarlane, Current Applied Physics 4 (2004) 389-393.

[56] W. Lu, A.G. Fadeev, B. Qi, E. Smela, B.R. Mattes, J. Ding, G.M. Spinks, J. Mazurkiewicz, D. Zhou, G.G. Wallace, D.R. MacFarlane, S.A. Forsyth, M. Forsyth, Science 297 (2002) 983-987.

[57] P.A. Basnayaka, M.K. Ram, E.K. Stefanakos, A. Kumar, Electrochim. Acta 92 (2013) 376-382.